the plant journal

SEB Society for Experimental Biology

The Plant Journal (2018) **94,** 469–484 doi: 10.1111/tpj.13868

A BAHD acyltransferase catalyzing 19-*O*-acetylation of tabersonine derivatives in roots of *Catharanthus roseus* enables combinatorial synthesis of monoterpene indole alkaloids

Inês Carqueijeiro[1], Thomas Dugé de Bernonville[1], Arnaud Lanoue[1], Thu-Thuy Dang[2], Christiana N Teijaro[3], Christian Paetz[4], Kevin Billet[1], Angela Mosquera[1,5], Audrey Oudin[1], Sébastien Besseau[1], Nicolas Papon[6], Gaëlle Glévarec[1], Lucía Atehortùa[5], Marc Clastre[1], Nathalie Giglioli-Guivarc'h[1], Bernd Schneider[4], Benoit St-Pierre[1], Rodrigo B. Andrade[3], Sarah E. O'Connor[2] and Vincent Courdavault[1,*]

[1]*EA2106 'Biomolécules et Biotechnologies Végétales', Université de Tours, Tours, France,*
[2]*Department of Biological Chemistry, The John Innes Centre, Norwich NR4 7UH, UK,*
[3]*Department of Chemistry, Temple University, Philadelphia, Pennsylvania 19122, USA,*
[4]*Max-Planck-Institute for Chemical Ecology, Beutenberg Campus, Hans-Knöll-Str. 8, D-07745 Jena, Germany,*
[5]*Laboratorio de Biotecnología, Universidad de Antioquia, Sede de Investigación Universitaria, Medellin, Colombia, and*
[6]*EA3142 'Groupe d'Etude des Interactions Hôte-Pathogène', Université d'Angers, Angers, France*

Received 28 September 2017; revised 13 December 2017; accepted 5 February 2018; published online 13 February 2018.
*For correspondence (e-mail vincent.courdavault@univ-tours.fr).

SUMMARY

While the characterization of the biosynthetic pathway of monoterpene indole alkaloids (MIAs) in leaves of *Catharanthus roseus* is now reaching completion, only two enzymes from the root counterpart dedicated to tabersonine metabolism have been identified to date, namely tabersonine 19-hydroxylase (T19H) and minovincine 19-*O*-acetyltransferase (MAT). Albeit the recombinant MAT catalyzes MIA acetylation at low efficiency *in vitro*, we demonstrated that MAT was inactive when expressed in yeast and *in planta*, suggesting an alternative function for this enzyme. Therefore, through transcriptomic analysis of periwinkle adventitious roots, several other BAHD acyltransferase candidates were identified based on the correlation of their expression profile with T19H and found to localize in small genomic clusters. Only one, named tabersonine derivative 19-*O*-acetyltransferase (TAT) was able to acetylate the 19-hydroxytabersonine derivatives from roots, such as minovincinine and hörhammericine, following expression in yeast. Kinetic studies also showed that the recombinant TAT was specific for root MIAs and displayed an up to 200-fold higher catalytic efficiency than MAT. In addition, gene expression analysis, protein subcellular localization and heterologous expression in *Nicotiana benthamiana* were in agreement with the prominent role of TAT in acetylation of root-specific MIAs, thereby redefining the molecular determinants of the root MIA biosynthetic pathway. Finally, identification of TAT provided a convenient tool for metabolic engineering of MIAs in yeast enabling efficiently mixing different biosynthetic modules spatially separated in the whole plant. This combinatorial synthesis associating several enzymes from *Catharanthus roseus* resulted in the conversion of tabersonine in tailor-made MIAs bearing both leaf and root-type decorations.

Keywords: acetyltransferase, BAHD acyltransferase, alkaloids, *Catharanthus roseus*, combinatorial biosynthesis, metabolic engineering, tabersonine.

INTRODUCTION

Numerous plants from the Apocynaceae, Loganiaceae and Rubiaceae families evolved a specialized metabolism leading to the synthesis of the poisonous monoterpene indole alkaloids (MIAs) that constitute a cornerstone of their defense arsenal (St-Pierre *et al.*, 2013). For decades, the inherent pharmacological properties of MIAs have been exploited to treat human diseases as exemplified with the antiarrhythmic drug ajmaline, the peripheral vasodilator raubasine and the highly valuable anti-cancer drugs vinblastine and vincristine (van Der Heijden *et al.*, 2004).

© 2018 The Authors
The Plant Journal © 2018 John Wiley & Sons Ltd

Amongst MIA-producing plants, the Madagascar periwinkle (*Catharanthus roseus*) is, by far, the most studied since it is still the sole source of the aforementioned antineoplastic MIAs. Over the last 60 years, many research groups have contributed to the elucidation of the MIA biosynthetic pathway and to its organization *in planta* making this complex specialized metabolism one of the best characterized to date (Courdavault *et al.*, 2014). Notably, most of this information relates to MIA biosynthesis in leaves, the main accumulation site of vindoline, a precursor of vinblastine/vincristine (Westekemper *et al.*, 1980). The formation of vindoline results from the seven-step conversion of tabersonine, beginning with C16 hydroxylation by tabersonine 16-hydroxylase (T16H2, CYP71D351), methylation of this hydroxyl group by 16-hydroxytabersonine 16-*O*-methyltransferase (16OMT) and a final acetylation by deacetylvindoline 4-*O*-acetyltransferase (DAT; St-Pierre *et al.*, 1998; Besseau *et al.*, 2013; Qu *et al.*, 2015) (Figure 1).

Interestingly, identification of DAT led to defining the class of acyltransferase known as BAHD acyltransferases (BAHDs) according to the name of initially characterized enzymes of this family (BEAT, benzylalcohol *O*-acetyltransferase; AHCT, anthocyanin *O*-hydroxycinnamoyltransferase; HCBT, anthranilate *N*-hydroxycinnamoyl/benzoyltransferase; DAT) (St-Pierre *et al.*, 1998; D'Auria, 2006). BAHDs constitute a large family of enzymes, with around 110 biochemically characterized members, catalyzing acyl-CoA dependent acylations of diverse specialized metabolites such as terpenoids, alkaloids or phenolics. Based on their overall identity, BAHDs have been successively clustered into eight distinct clades displaying either strict of less stringent specifies for CoA thioester donor and for substrates (D'Auria, 2006; Luo *et al.*, 2007; Yu *et al.*, 2009; Tuominen *et al.*, 2011).

Although MIA biosynthesis is well characterized in *C. roseus* leaves, data concerning MIA metabolism in roots are scarce. Roots accumulate diverse MIA structural classes such as the iboga-type catharanthine, the heteroyohimbine, ajmalicine and serpentine and various aspidosperma MIAs including the tabersonine derivatives 19-*O*-acetylhörhammericine and echitovenine (Laflamme *et al.*, 2001; Ferreres *et al.*, 2010). Enzymes involved in heteroyohimbine synthesis have been recently described (Stavrinides *et al.*, 2015, 2016). The synthesis of 19-*O*-acetylhörhammericine and echitovenine results from three sequential reactions involving either a 6,7-epoxidation or 6,7-reduction, a C19 hydroxylation and 19-*O*-acetylation (Figure 1). While the precise reaction sequence has not been solved, two enzymes from this pathway have been described: tabersonine 19-hydroxylase (T19H, CYP71BJ1) and minovincinine 19-hydroxy-*O*-acetyltransferase (MAT) (Laflamme *et al.*, 2001; Giddings *et al.*, 2011). In addition, an activity for 6,7-epoxidation has been characterized as a P450 enzyme (Rodriguez *et al.*, 2003).

With the aim to initiate the bio-engineered production of root MIAs in heterologous organisms as reported for strictosidine and vindoline (Miettinen *et al.*, 2014; Brown *et al.*, 2015; Qu *et al.*, 2015), we reinvestigated in this work the acetylation reactions of 19-hydroxytabersonine derivatives. This led to the identification of TAT, a 19-*O*-acetyltransferase displaying high activity on tabersonine derivatives in yeast and in plants as compared to MAT. Furthermore, combining TAT with previously identified MIA biosynthetic enzymes ultimately allowed the engineered synthesis of unnatural tabersonine derivatives. Such a system thus constitutes a valuable tool to perform tailor-made decorations of the tabersonine scaffold yielding potential anti-cancer or anti-Alzheimer compounds (Lim *et al.*, 2008; Frei *et al.*, 2013; Kai *et al.*, 2015; Chung *et al.*, 2017).

RESULTS

Efficient expression of MAT in yeast cells did not allow biotransformation of 19-hydroxylated tabersonine derivatives into acetylated products

To initiate the bioconversion of tabersonine into the root-specific MIAs, yeast strains expressing T19H and MAT or MAT alone were first generated using autoreplicative plasmids bearing inducible promoters. Sequencing of the cloned cDNAs revealed that both gene sequences were strictly identical to the published ones (Laflamme *et al.*, 2001; Giddings *et al.*, 2011). Galactose-induced transformed yeast cultures were then fed with tabersonine (125 μM) for 24 h and the resulting products were analyzed by UPLC-MS (Figure 2(a)). T19H expression resulted in substantial bioconversion of tabersonine into 19-hydroxytabersonine (m/z 353). In contrast, no acetylated form of this compound (m/z 395) was observed when MAT was co-expressed along with T19H. In these cells, although 19-hydroxytabersonine was formed, it was not consumed (Figure S1(a)). As a control, we confirmed that MAT mRNAs accumulated (Figure 2(b)) and MAT protein was present (Figure 2(c)). Since MAT activity has never been reported to acetylate 19-hydroxytabersonine, assays were also performed with previously reported MAT substrates (Figure 1). Vincadifformine was properly hydroxylated by T19H into minovincinine, but no further conversion occurred suggesting that MAT did not acetylate minovincinine in yeast (Figure 2(a)). Deacetylvindoline and hörhammericine were also tested; however, the expected acetylated products vindoline (m/z 457) and 19-acetylhörhammericine (m/z 411) were neither detected in the yeast culture medium (Figure 2(a)) nor inside yeasts (Figure S1(b)). Due to the relatively high K_m of MAT for MIAs (120 to 250 μM, Laflamme *et al.*, 2001), additional assays were conducted with 500 μM of tabersonine derivatives but again no acetylated products were observed (Figure S1(c)). In addition, feeding yeast cells with acetylated MIAs such as vindoline did not reveal any endogenous

© 2018 The Authors

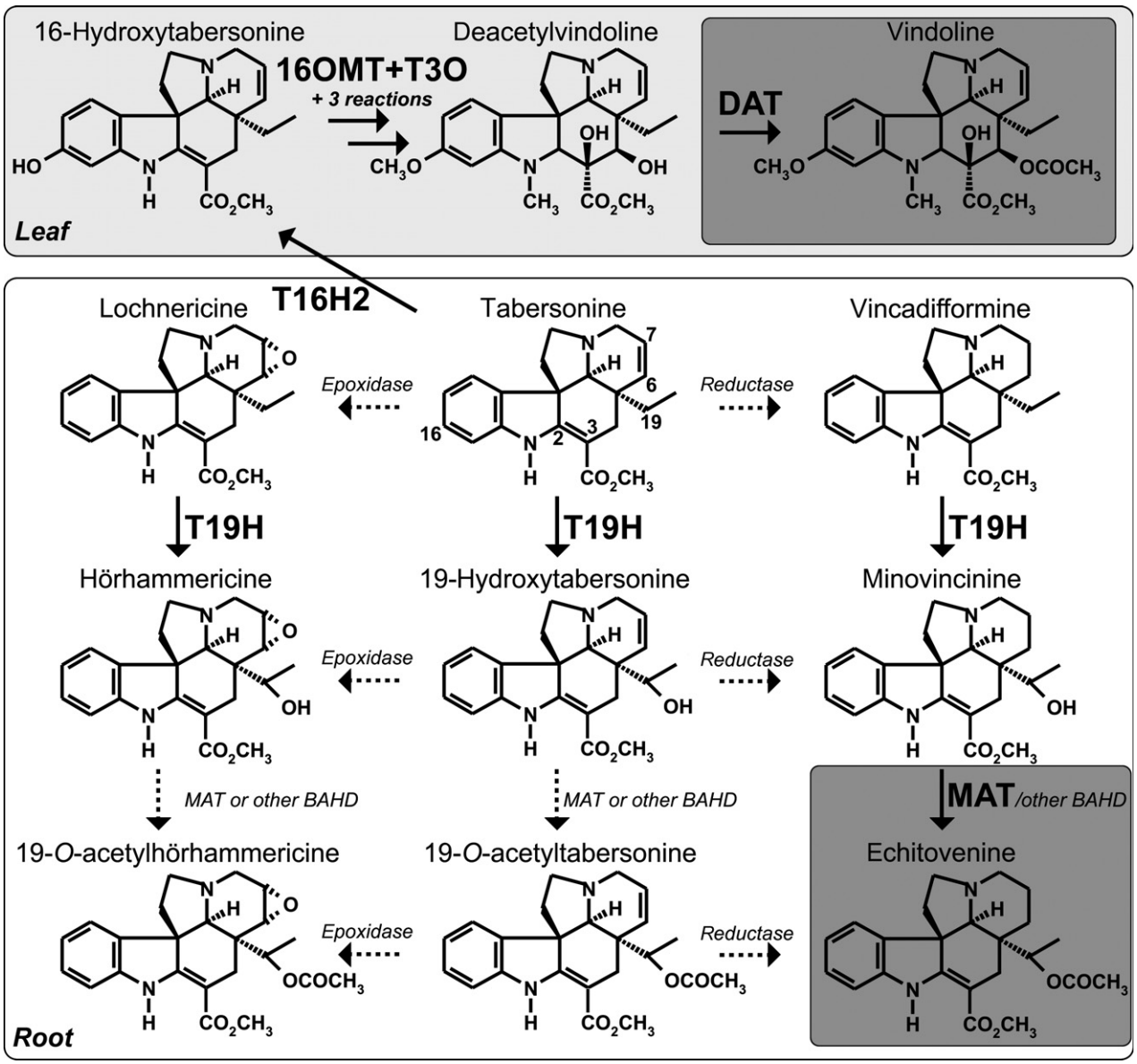

Figure 1. The biosynthetic pathway of tabersonine derivatives in root and leaves of *C. roseus*.
Solid and dashed arrows represent characterized and uncharacterized reactions, respectively. Reactions catalyzed by characterized BAHD (DAT and MAT) are highlighted in dark gray. T16H2, tabersonine 16-hydroxylase 2; T3O, tabersonine 3-oxydase; T19H, tabersonine 19-hydroxylase, DAT, deacetylvindoline 4-*O*-acetyltransferase; MAT, minovincinine 19-hydroxy-*O*-acetyltransferase; 16OMT, 16-hydroxytabersonine 16-*O*-methyltransferase. Positions of the carbon atoms subjected to modification are numerated.

esterase activity that could potentially hydrolyze acetylated products (Figure S1(d)). These results thus prompt us to search for alternative BAHDs in *C. roseus* that may efficiently acetylate 19-hydroxytabersonine derivatives *in vivo*.

RNA-seq analyses combined to expression correlation studies with T19H led to identification of BAHD acyltransferase candidates expressed in roots

While we first established that roots from *C. roseus* had a high level of 19-*O*-acetyltransferase activity, which is in agreement with their MIA content (Figure S2(a–c)), analysis of the previously generated transcriptomic data from this organ revealed a low abundance of MIA biosynthetic transcripts (Figure S3(a) and Figure S4). As these resources might not be adequate to conduct sensitive gene expression correlation studies, we initiated adventitious roots from *C. roseus* stems to generate additional transcriptomic resources (Figure S2(b)). A uniform population of young roots was conveniently collected to perform RNA sequencing. Following transcriptome reconstitution and analysis (Figure S4 – ERR2112587 accession number, Table S1), we

© 2018 The Authors
The Plant Journal © 2018 John Wiley & Sons Ltd,

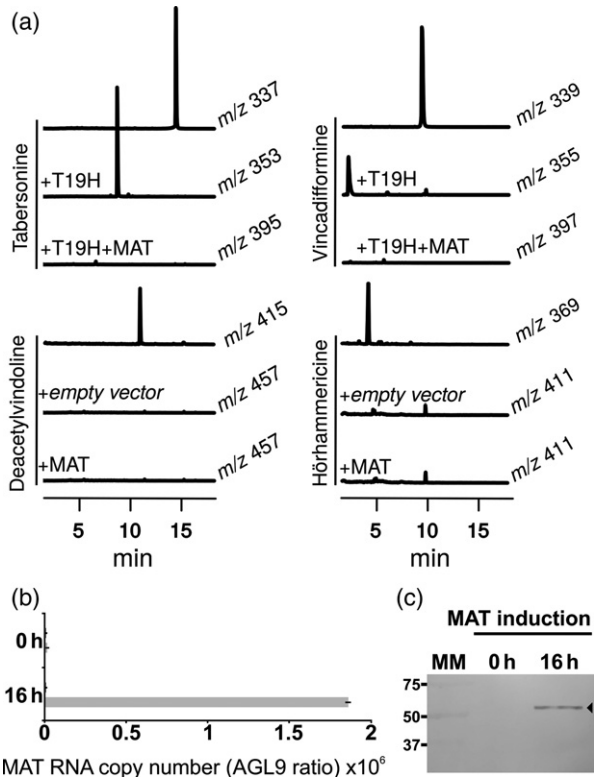

Figure 2. MAT does not acetylate root tabersonine derivatives or deacetylvindoline when expressed in yeast.
(a) LC-MS chromatograms using selected ion monitoring of the reaction products of yeast cell cultures expressing either T19H, T19H and MAT, MAT or containing an empty vector, incubated with tabersonine, vincadifformine, hörhammericine or deacetylvindoline.
(b) The expression of the MAT transgene in yeast was determined by real-time RT-PCR performed before and after a 16 h galactose induction.
(c) Detection of the MAT protein by western blot analysis performed using anti-FLAG antibodies.

confirmed the high expression of MIA biosynthetic genes in adventitious roots (Figure S3(b)).

With a transcriptomic data set including adventitious root (this study), leaves (Dugé de Bernonville *et al.*, 2017) and other available data sets, Pearson correlation coefficients (PCC) with T19H were calculated on expression levels obtained after mapping reads to *C. roseus* transcripts predicted from genome sequence (Kellner *et al.*, 2015a) (Figure 3(a)). Within the members of the BAHD acyltransferase family retrieved from this analysis, five potential candidates displayed a strong correlation with T19H (PCC >0.8): CRO_T005210, CRO_T005211, CRO_T005215, CRO_T020281 and CRO_T0022100 as well as MAT (CRO_T005213) that exhibited the weaker correlation (0.82). As expected, DAT (CRO_T020280), involved in leaf alkaloid metabolism, was negatively correlated (PCC = −0.38). Interestingly, all BAHD candidates but CRO_T0022100 were located within two distinct gene clusters (Figure S5). Transcript profiling showed that the new BAHD candidates were mainly expressed in roots with higher level in the adventitious root (Root_AS) sample, in contrast to DAT expressed in leaves (Figure 3(b)). We noted that MAT and CRO_T022100 transcripts were also present in leaves and induced by methyljasmonate treatments but not the other candidates. Overall, the expression profiles of the BAHD candidates were similar to that of T19H reinforcing their potential involvement in tabersonine derivative acetylation. Phylogenetic analyses revealed that these candidates belong to clade IIIa of the BAHD superfamily that includes many enzymes involved in alkaloid metabolism (Figure S6 and Table S3). Except for the closely related CRO_T005210 and CRO_T020281 (91%), the newly identified BAHDs shared an average amino-acid identity of 48–56% and a similar level of identity with DAT and MAT (48–54%) while MAT has a higher similarity with DAT (77%) (Figure S7 and Table S2). All these proteins also conserved the characteristic amino-acid motifs of BAHD acyltransferases: the HXXXD residues in the central part of the protein shown to be involved in reaction catalysis; and at the C-terminal end, the DFGWG motif suggested to play a structural role (Figure S7; Ma *et al.*, 2005; D'Auria, 2006). However, a mutation of the tryptophan residue in the highly conserved DFGWG motif was observed in MAT, CRO_T020281 and CRO_T005210. Finally, consensus type I peroxisome targeting sequences (PTS1) were also detected in the last three residues of CRO_T005210, CRO_T005211, CRO_T020281 and CRO_T020282 strongly suggesting that these proteins can be addressed to peroxisomes (Reumann *et al.*, 2016). Such subcellular compartmentation was confirmed for CRO_T005210 by expression of YFP fusion proteins in *C. roseus* cells (Figure S8).

CRO_T005215 encodes a functional tabersonine derivative 19-*O*-acetyltransferase

To test the capacity of BAHD candidates to acetylate 19-hydroxy tabersonine derivatives, proteins were co-expressed with T19H or expressed individually in yeast, except for CRO_T05211 that we were not able to amplify probably due to a very low level of expression (Figure 3(b)). No conversion of 19-hydroxytabersonine, hörhammericine and minovincinine was observed with CRO_T005210, CRO_ T022100, CRO_T020281, MAT and DAT. By contrast, co-expression of CRO_T005215 caused a pronounced consumption of these compounds (Figures 3(c) and Figure S9(a–c)) accompanied by the appearance in the culture medium of products displaying retention times and mass-to-charge ratios consistent with 19-acetyltabersonine (m/z 395), 19-acetylhörhammericine (m/z 411) or echitovenine (m/z 397) (Figure 1). Furthermore, we noted that deacetylvindoline was acetylated by DAT, but not by the other enzymes, suggesting the existence of marked substrate specificities for the tested BAHD. To firmly identify the nature of the modification catalyzed

© 2018 The Authors

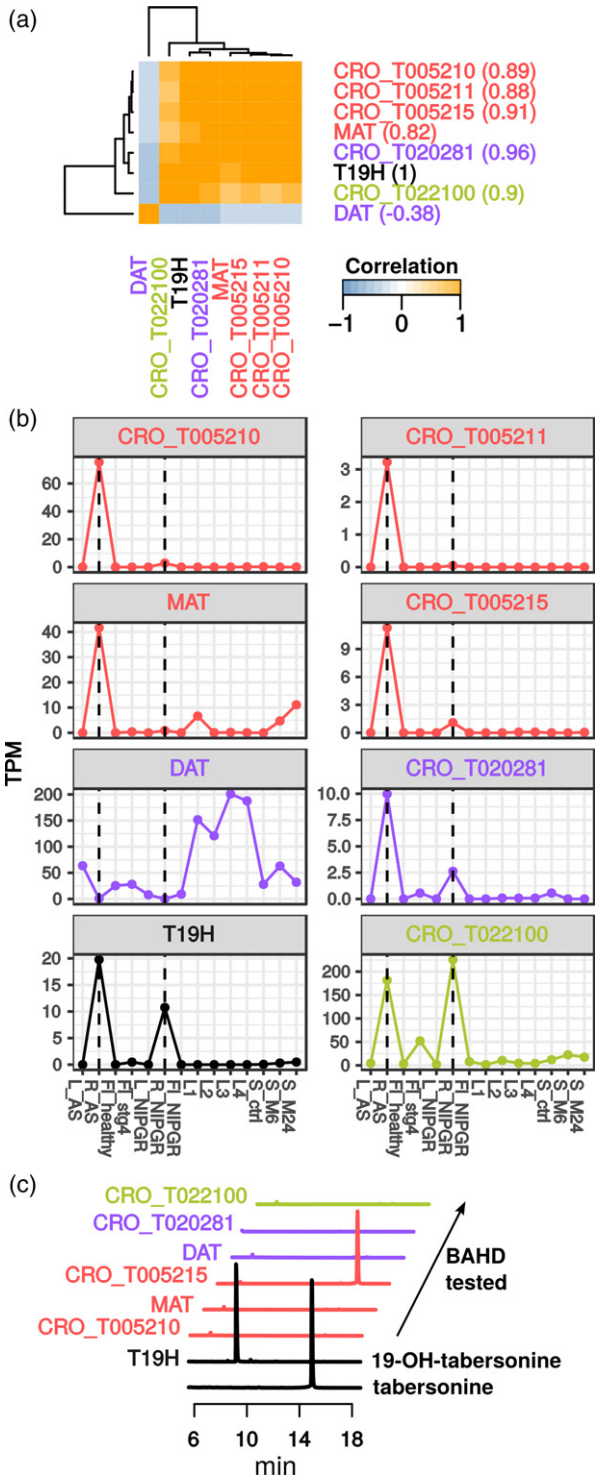

Figure 3. Identification of a BAHD acyltransferase acetylating tabersonine derivatives in yeast.
(a) Identification of candidate BAHD acyltransferases displaying the highest gene expression correlation with T19H – DAT (CRO_T020280) is given as a control. Pearson correlation coefficients were calculated using expression levels from pre-existing transcriptomics resources from leaves (L), flowers (Fl), shoots (S, control and MeJA treated), roots (R) and new data from adventitious roots (R_AS). Accession numbers of these resources are given in Figure S3. Dendrograms were constructed using Euclidean distance and complete agglomeration method.
(b) Expression profiles of the selected BAHD acyltransferases and T19H in the same samples.
(c) LC-MS chromatograms using selected ion monitoring of the reaction products of yeast cell cultures co-expressing T19H and the selected BAHD acyltransferases incubated with tabersonine. *m/z* 395, 19-acetyltabersonine. Color code highlights genes belonging to a same genomic scaffold (Figure S5).

by CRO_T005215, nuclear magnetic resonance (NMR) spectroscopy of the product confirmed the attachment of the acetyl group to C-19 (Figure S10). This establishes the regioselectivity of CRO_T005215 in the 19-*O*-acetylation of 19-hydroxytabersonine and most likely for 19-*O*-acetylation of hörhammericine and minovincinine as well. As a consequence, CRO_T005215 was named tabersonine derivative 19-*O*-acetyltransferase (TAT; GenBank accession number KU821123).

In vitro, recombinant MAT and TAT acetylate 19-hydroxytabersonine derivatives but TAT displays a much higher catalytic efficiency

In order to gain insight into TAT enzymatic specificities and the lack of MAT *in vivo* activity, the biochemical properties of both enzymes were subsequently evaluated following their heterologous expression and purification in *E. coli* (Figure S11(a)). In contrast to *in vivo* assays in yeast, recombinant purified MAT protein displayed acetyltransferase activity *in vitro*, as previously reported (Table 1; Laflamme *et al.*, 2001). As expected, TAT recombinant protein was also active *in vitro*. Kinetic parameters of the recombinant proteins were determined with acetyl-CoA as acyl donor and with various acyl acceptors: 19-hydroxytabersonine, hörhammericine, minovincinine, deacetylvindoline and also non-related MIA compounds such as spermidine, quercetin, cyanidin, naringenin and caffeic acid (Table 1). First, we noted that MAT and TAT were not able to acetylate compounds outside of the MIA family, suggesting that both enzymes are specific to 19-hydroxytabersonine derivatives. In agreement, deacetylvindoline, a 16-hydroxylated tabersonine derivative, was not an acetyl acceptor. Furthermore, steady-state analyses highlighted differences in kinetic parameters of TAT and MAT. For instance, TAT exhibited a low K_m (9 μM) for minovincinine while it reached 58 μM and 78 μM for hörhammericine and 19-hydroxytabersonine, respectively. By contrast, MAT displayed nearly similar K_m values for the three compounds ranging from 21 μM for minovincinine to 40 μM for 19-hydroxytabersonine. Most importantly, TAT exhibited *k*cat values around 50-fold (19-hydroxytabersonine), 65-fold (minovincinine) and up to 230-fold (hörhammericine) higher than those of MAT. Accordingly, TAT catalytic efficiencies ($k$cat/K_m) were much higher than MAT, from 20-fold (19-hydroxytabersonine), 80-fold (hörhammericine) to 200-fold (minovincinine). In addition, specificity for CoA donors was also investigated

© 2018 The Authors

by testing acylation of 19-hydroxytabersonine with acetyl-CoA, benzoyl-CoA, cinnamoyl-CoA, *p*-coumaroyl-CoA, caffeoyl-CoA, feruloyl-CoA and sinapoyl-CoA donors (Table 1). In our experimental conditions, TAT and MAT exclusively used acetyl-CoA as a donor, establishing their high specificity towards the acyl donor. Both enzymes exhibited similar K_m values (around 5 μM) but again TAT differed from MAT by a 100-fold higher *k*cat.

Interestingly, mutation analyses revealed that the tryptophan to leucine substitution in the highly conserved DFGWG motif of TAT, and the reverse substitution to establish the conserved motif in MAT, have no consequence on TAT and MAT activities, respectively (Figure S7 and Figure S11(b, c)). Furthermore, incubating 19-acetyltabersonine with CoA revealed that neither TAT and MAT nor their mutated versions carry out deacetylation reaction in contrast to the well characterized vinorine synthase (VS) from *Rauwolfia serpentina* (Bayer *et al.*, 2004) (Figure S11 (d)). Taken together, our results demonstrate that both TAT and MAT specifically acetylate tabersonine derivatives *in vitro* in the forward reaction with TAT exhibiting a much higher catalytic efficiency. The lack of *in vivo* activity of MAT in recombinant yeast may be related to its low catalytic activity towards tabersonine derivatives.

TAT displays gene expression features relevant to a prominent role in tabersonine acetylation in roots of *C. roseus*

To study the function of TAT *in planta*, we investigated the expression profile of TAT and MAT in *C. roseus* organs. Since 19-hydroxylation occurs necessarily before 19-*O*-acetylation, the expression of the specific BAHD is expected to be correlated to both T19H expression profile and to 19-*O*-acetylated MIA accumulation.

We first confirmed that TAT transcripts followed an expression pattern similar to T19H with a main accumulation in roots in agreement with our transcriptomics results (Figure 4(a)). Such expression profiles differed from those of MAT and DAT for which transcripts were also detected or mainly accumulated in leaves, respectively. In addition, we also compared TAT and MAT expression in hairy roots and in adventitious roots induced from stem cuttings. Biosynthesis of tabersonine derivatives was active in adventitious roots but downregulated in hairy roots (Figure 4(b)). A single acetylated tabersonine derivative was present in adventitious roots, namely echitovenine, while it was barely detectable in hairy roots. While TAT was expressed in both types of roots, the 50-fold up-regulation of MAT in hairy roots and the low expression in adventitious roots appear to be disconnected with the acetylated tabersonine metabolism in these organs (Figure 4(c)). These expression profiles thus argue for a prominent role of TAT in 19-*O*-acetylation of tabersonine derivatives in *C. roseus* roots compared to MAT. Such a concerted reaction of T19H and TAT is also facilitated by their close subcellular compartmentation in the cell relying on the anchoring of T19H to the endoplasmic reticulum (ER) and on the nucleocytosolic distribution of TAT contributing to product/substrate channeling as suggested by subcellular localization studies of fusion to fluorescent proteins (Figure S12(a–u)).

Table 1 Kinetic parameters of acetylation activity of the recombinant TAT and MAT

		MAT	TAT
CoA-donor	Acetyl-CoA	K_m 6 ± 0.5 μM; V_{max} 0.014 ± 0.001 μM sec^{-1}; k_{cat} 0.014 ± 0.001 sec^{-1}; k_{cat}/K_m 2.5 × 10^3 $sec^{-1}.M^{-1}$	K_m 5 ± 0.5 μM; V_{max} 0.14 ± 0.007 μM sec^{-1}; k_{cat} 1.44 ± 0.07 sec^{-1}; k_{cat}/K_m 2.6 × 10^5 $sec^{-1}.M^{-1}$
	Benzoyl-CoA	–	–
	Cinnamoyl-CoA	–	–
	p-Coumaroyl-CoA	–	–
	Caffeoyl-CoA	–	–
	Feruloyl-CoA	–	–
	Sinapoyl-CoA	–	–
Substrates	Quercetin	–	–
	Naringenin	–	–
	Cyanidin	–	–
	Caffeic acid	–	–
	Spermidine	–	–
	19-OH Tabersonine	K_m 40 ± 6 μM; V_{max} 0.25 ± 0.03 μM.sec^{-1}; k_{cat} 0.26 ± 0.03 sec^{-1}; k_{cat}/K_m 6.5 × 10^3 $sec^{-1}.M^{-1}$	K_m 78 ± 4 μM; V_{max} 1.32 ± 0.09 μM.sec^{-1}; k_{cat} 13.2 ± 0.98 sec^{-1}; k_{cat}/K_m 1.7 × 10^5 $sec^{-1}.M^{-1}$
	Hörhammericine	K_m 21 ± 6 μM; V_{max} 1 × 10^{-4} ± 1 × 10^{-5} μM.sec^{-1}; k_{cat} 0.001 ± 1 × 10^{-4} sec^{-1}; k_{cat}/K_m 47 $sec^{-1}.M^{-1}$	K_m 58 ± 3 μM; V_{max} 0.02 ± 7 × 10^{-4} μM.sec^{-1}; k_{cat} 0.23 ± 0.007 sec^{-1}; k_{cat}/K_m 3.9 × 10^3 $sec^{-1}.M^{-1}$
	Minovincinine	K_m 28 ± 3 μM; V_{max} 0.001 ± 0.0003 μM.sec^{-1}; k_{cat} 0.02 ± 0.002 sec^{-1}; k_{cat}/K_m 710 $sec^{-1}.M^{-1}$	K_m 9 ± 0.3 μM; V_{max} 0.13 ± 0.001 μM.sec^{-1}; k_{cat} 1.31 ± 0.01 sec^{-1}; k_{cat}/K_m 1.47 × 10^5 $sec^{-1}.M^{-1}$

His-tagged TAT and MAT were expressed in *E. coli*, purified and assayed for acylation activity. Kinetic parameters were determined as described under the experimental procedure section. The results are the mean of three independent assays. '–', no detectable activity.

© 2018 The Authors

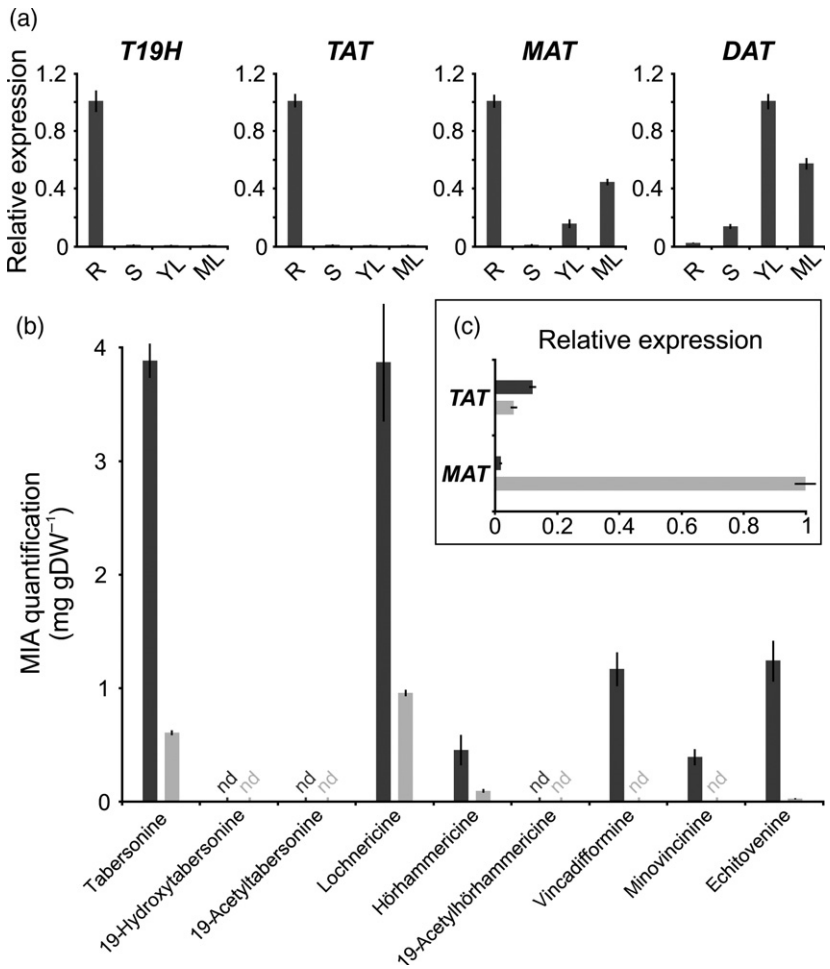

Figure 4. Analysis of TAT transcript distribution and MIA accumulation in *C. roseus* organs, hairy roots and adventitious roots.
(a) *T19H* and *TAT* are exclusively expressed in roots in contrast to *MAT* and *DAT*. The relative expression of each gene was determined by real-time RT-PCR analyses performed on RNA extracted from various *C. roseus* organs (R, roots; S, stems; YL, young leaves; ML, mature leaves).
(b) Relative quantification of the main tabersonine derivatives in *C. roseus* adventitious roots (dark gray) and hairy roots (light gray) performed by UPLC-MS analysis (nd, not detected).
(c) The relative amounts of TAT and MAT transcripts were quantified by qPCR. Adventitious roots (dark gray) and hairy roots (light gray) were extracted simultaneously for both alkaloid and RNA. Data represent mean ± standard error (SE) of three technical replicates performed individually on six samples of each organ type. *RPS9* and *ERF1α* were used as reference genes.

We next attempted to downregulate TAT gene expression in *C. roseus* roots by virus-induced gene silencing (VIGS). Although VIGS is an efficient system to downregulate gene expression in leaf, TAT expression in roots was found to be recalcitrant to downregulation (Figure S13 (a–f)). As a consequence, we conducted *in planta* assays by overexpressing TAT and MAT in leaves of *Nicotiana benthamiana* (Figure 5). After cloning TAT and MAT coding sequences into the binary plasmid pCAMBIA1302 to express the TAT–GFP and MAT–GFP fusion proteins, recombinant plasmids or empty pCAMBIA1302 were individually agroinfiltrated in young leaves. Analysis of GFP fusion protein expression confirmed that the number of cells producing GFP, TAT–GFP and MAT–GFP were almost equivalent suggesting no biases in levels of protein expression (Figure 5(a–f)). Both TAT–GFP and MAT–GFP fusion proteins also exhibited a similar subcellular localization and a similar size as revealed by western blot analysis (Figure 5(g–l)). For studying acetyltransferase activity, leaf disks from each transformed area were excised and vacuum-infiltrated with buffer containing minovincinine and acetyl-CoA. In these conditions, only the TAT–GFP fusion protein was shown to acetylate minovincinine while GFP and MAT–GFP did not (Figure 5(k)). Such specificity was confirmed by conducting a similar assay in yeast, which also demonstrated that substrate accessibilities were not limiting MAT activity (Figure S14(a–n)). All the results thus suggest that TAT displays a prominent role in 19-*O*-acetylation of tabersonine derivatives *in planta* and potentially constitutes a promising tool for the metabolic engineering of the MIAs from *C. roseus* roots.

TAT allows metabolic engineering of yeast for production of unnatural MIAs

In planta, leaf and root have distinct metabolisms of tabersonine as a result of organ-specific expression of several genes involved in the leaf-borne vindoline pathway and in 19-acetyltabersonine/19-acetylhörhammericine/echitovenine pathways in roots. We hypothesized that combining selected enzymes from these pathways in a yeast expression platform might allow the production of non-natural MIAs.

In the vindoline pathway, tabersonine is subjected to two distinct regio-specific modifications: (i) C16 hydroxylation and methylation by T16H2 and 16OMT to form

© 2018 The Authors

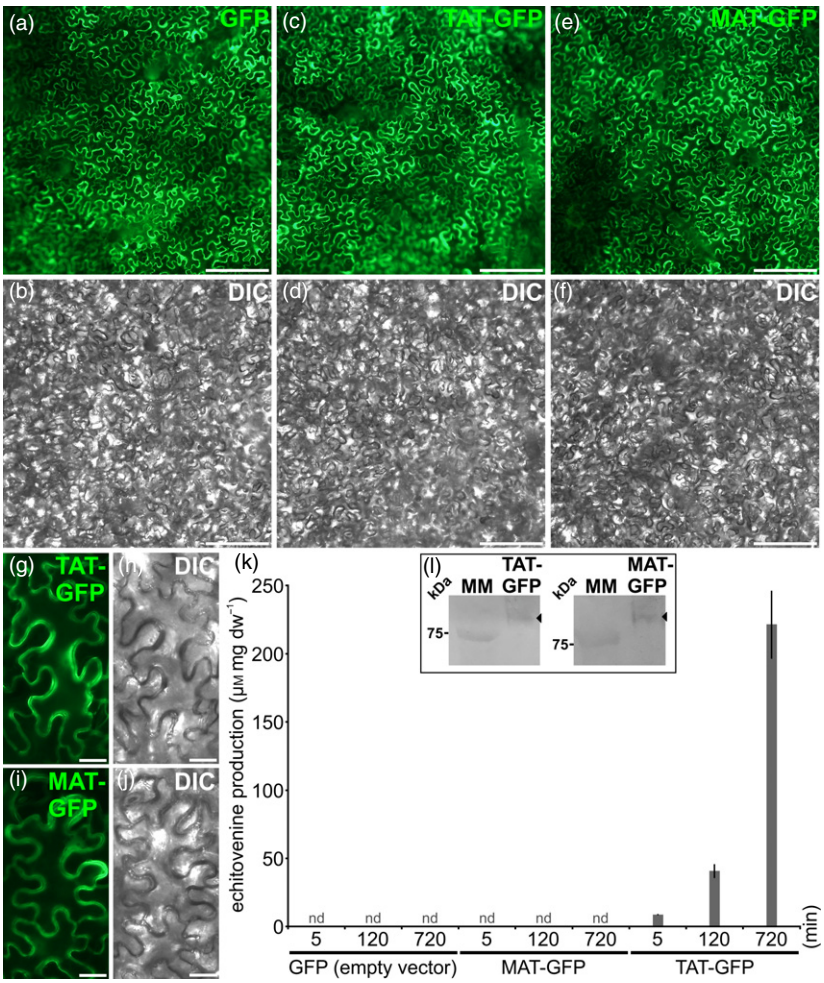

Figure 5. TAT but not MAT acetylates minovincinine in leaves of *N. benthamiana*.
(a–j) GFP (a, b), TAT–GFP (c, d, g, h) and MAT–GFP (e, f, i, j) were transiently overexpressed in *N. benthamiana* leaves through agrotransformations during 5 days before observation. Bars, 100 μm (a–f); 10 μm (g–j). DIC, differential interference contrast.
(k) Infiltrated areas expressing the fusion proteins were harvested and infiltrated with minovincinine and acetyl-CoA during 5, 120 or 720 min before estimation of acetyltransferase activity through echitovenine quantification.
(l) TAT–GFP and MAT–GFP were detected by western blot analysis performed using anti-GFP antibodies.

16-methoxytabersonine; (ii) C2–C3 epoxidation by tabersonine 3-oxidase (T3O) yielding to 16-methoxytabersonine epoxide/imine alcohol when this reaction is performed on 16-methoxytabersonine or to tabersonine epoxide when T3O acts directly on tabersonine (Levac *et al.*, 2008; Besseau *et al.*, 2013; Kellner *et al.*, 2015b; Qu *et al.*, 2015) (Figure 6(a)). We first attempted to combine C3 (leaf specific) and C19 (root-specific) modifications of tabersonine. When expressed separately, both T19H and T3O were able to convert tabersonine into the expected compounds that displayed the same *m/z* (353) but different retention times (Figure 6(b)). However, in yeasts co-expressing both T19H and T3O, neither 19-hydroxy tabersonine epoxide nor the corresponding imine alcohol that can be spontaneously formed following epoxide opening (predicted *m/z* 369) were detected. Careful examination of the reaction products showed the presence of 19-hydroxytabersonine and the preferential accumulation of tabersonine epoxide confirming that both T19H and T3O were active but also demonstrated that these two modifications of tabersonine cannot occur simultaneously on the same molecule. We then tested combination of C16 (leaf specific T16H2 and 16OMT) and C19 (root-specific T19H and TAT) modifications of tabersonine (Figure 6(a, c)). As compared to control cells, we first established that co-expressing T16H2 and 16OMT led to the expected successive conversion of tabersonine into 16-hydroxytabersonine (*m/z* 353) and 16-methoxytabersonine (*m/z* 367). Interestingly, addition of T19H to this strain induced the formation of a more hydrophilic compound with *m/z* 383 consistent with the expected 16-methoxy-19-hydroxytabersonine. Furthermore, the addition of the TAT gene to the system resulted in synthesis of a more hydrophobic product (m/z 425) that is consistent with the acetylation of 16-methoxy-19-hydroxytabersonine to 16-methoxy-19-acetyltabersonine (Figures 6(a, c) and S15). Besides accumulation of several biosynthetic intermediates, the final conversion into this last compound reached around 10% of the starting amount of tabersonine after 16 h of incubation with the yeast culture (around 106 ± 20 μg.g DW^{-1}). Interestingly, all the biotransformed MIAs and biosynthetic intermediates were secreted in the culture medium leaving behind only trace levels within

© 2018 The Authors

yeasts (Figure S1(e)). Altogether, these results strongly suggest that tabersonine can be simultaneously decorated on the distal regions C16 and C2–C3, to form 16-methoxytabersonine epoxide, which is naturally observed in the vindoline pathway, C16 and C19 to generate the new-to-*C. roseus* compound 16-methoxy-19-hydroxytabersonine, and that simultaneous decorations of C2–C3 and C19 are not compatible. Similar conversions were obtained when vincadifformine or hörhammericine are used as the starting substrate leading to the synthesis of several unnatural MIAs including 16-methoxy-echitovenine from vincadifformine and 16-methoxy-19-acetylhörhammericine from hörhammericine (Figure S16(a–c) and Figure S17(a, b)). Our results therefore demonstrate that MIA biosynthetic enzymes can be used as tools to synthesize tailor-made MIAs via mixing distinct enzyme modules. As such, the synthesis of 16-methoxy-19-acetyltabersonine in yeast through the expression of four plant genes constitutes a proof of principle for metabolic engineering of *C. roseus* root MIAs in a heterologous organism and is also an example of a streamlined enzyme combination allowing a controlled reorientation of the synthetic fluxes.

DISCUSSION

MAT has minor or indirect role in 19-*O*-acetylation of tabersonine derivatives

Over the last 5 years, the elucidation of the MIA biosynthetic pathway in *C. roseus* has progressed tremendously and has allowed the development of bioengineering strategies leading to the production of MIAs in heterologous organisms such as *N. benthamiana* or *S. cerevisiae* (Courdavault *et al.*, 2014; Miettinen *et al.*, 2014; Brown *et al.*, 2015; Qu *et al.*, 2015). Most of these advances essentially apply to the early steps of MIA synthesis up to strictosidine, the universal MIA precursor, or to MIAs restricted to the aerial parts of the plant. By contrast, the characterization of MIA biosynthesis in roots has retained only limited attention and no metabolic engineering approach has emerged. Up to now, two root-specific enzymes have been identified, T19H performing the hydroxylation of tabersonine (Giddings *et al.*, 2011) and MAT, a BAHD described to catalyze the acetylation reaction in the synthesis of 19-O-acetylhorhammericine and echitovenine (Laflamme *et al.*, 2001). However, all our results tend to demonstrate that MAT only displays a very low catalytic efficiency *in vitro* towards root tabersonine derivatives (Table 1) in agreement with Laflamme *et al.* (2001). Such a low efficiency is unlikely to arise from uses of an incorrect acyl donor since the recombinant MAT has a low K_m towards acetyl-CoA, precluding other possible reactions of acylation that could lead to other MIAs such as 16-methoxyechitovenilline, acylated by trimethoxy benzoyl in *Alstonia venenata* (Majumder *et al.*, 1979). The low catalytic efficiency of MAT also does not result from the absence of tryptophan in the DFGWG domain since restoration of this amino acid in a mutant MAT does not improve catalytic activity, in contrast to the pronounced effect of the D mutation (xFGWG) on BAHD activity (Figure S7 and Figure S11(c); Bayer *et al.*, 2004; Tuominen *et al.*, 2011). Furthermore, this low catalytic efficiency *in vitro* correlates with the lack of detectable MAT activity *in vivo* as established in yeast *and N. benthamiana* (Figure 2, 5 and Figure S14). While we cannot exclude that our *in vivo* assays were not sensitive enough to measure rare acetylations, we established that this lack of activity did not result from protein degradation or altered subcellular localization as revealed by western blot analysis and GFP imaging in yeast or *N. benthamiana* cells (Figures 5 and S14). It neither resulted from high endogenous esterase activities that could overcome the low acetyltransferase activity of MAT since no de-esterification of acetylated MIAs has been measured (Figure S1(d)). Although MAT inactivity *in vivo* may result from inhibitions caused by the abundant presence of other proteins in the whole cell as previously suggested (Magnotta *et al.*, 2007), MAT low catalytic activity *in vitro* might also represent the persistence of an ancient acyltransferase activity that evolved to acetylate other yet unknown MIAs *in planta* exhibiting a tabersonine- or other- type backbone. Altogether, these results thus strongly suggest that MAT has a minor or no direct role in acetylation of tabersonine derivatives in roots of *C. roseus*.

TAT displays biochemical properties and gene expression profiles consistent with a prominent role in tabersonine derivative acetylation

Through the development of a transcriptomic resource from *C. roseus* adventitious roots (Figure S3 and Figure S4), analysis of gene expression correlation led to the identification of TAT (CRO_T005215) as an enzyme catalyzing the 19-*O*-acetylation of tabersonine derivatives *in vivo* (Figures 3(c), 5, S9 and S12).

At the biochemical level, TAT displays a K_m value in the μM range like the other BAHDs involved in MIA biosynthesis such as DAT and VS of *R. serpentina*, (this work; Laflamme *et al.*, 2001; Bayer *et al.*, 2004). However, the recombinant enzyme has marked differences in affinity for the tested substrates with a lower K_m for minovincinine (9 μM) and a roughly six-fold to eight-fold higher K_m for 19-hydroxytabersonine and hörhammericine. This indicates that the C6–C7 configuration of the tabersonine backbone has marked consequences on TAT enzyme affinity. Presence of an epoxide or a double bound at this position probably changes substrate conformation and/or increases steric hindrance in the C5–C6 region resulting in affinity decreasing and by consequence in a marked preference for saturated bond. Such kind of specificity has already been reported for the acetyl-ajmalan esterase that hydrolyzes

© 2018 The Authors

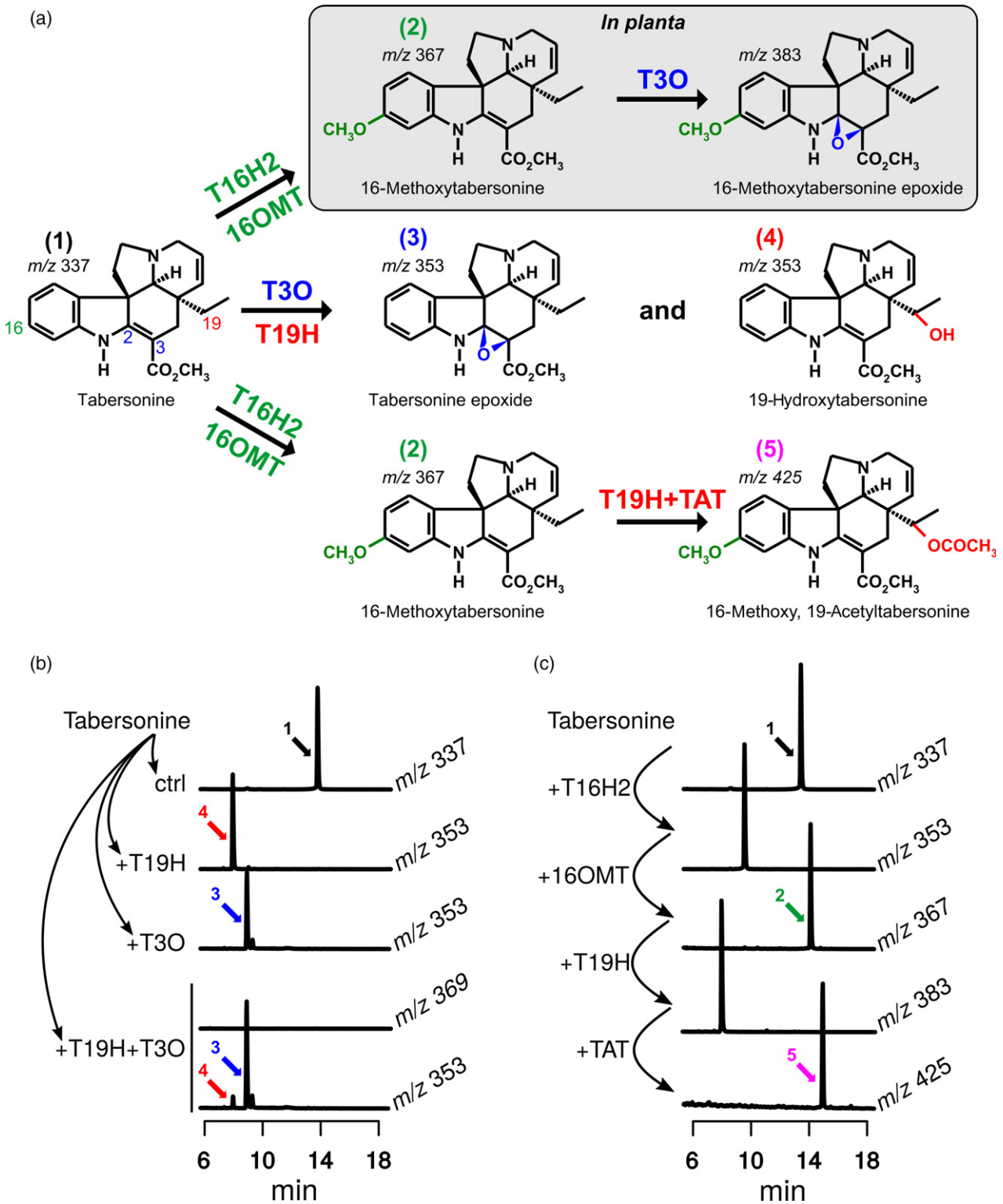

Figure 6. Combining enzymes from roots and leaves in yeast allows the synthesis of new-to-*C. roseus* MIAs.
(a) Combinatorial association of *C. roseus* MIA biosynthetic enzymes from roots (T19H, TAT) and leaves (T16H2, 16OMT, T3O) and formation of MIAs.
(b) Co-expression of T3O and T19H in yeast fed with tabersonine does not lead to the synthesis of 19-hydroxytabersonine epoxide but only to the formation of 19-hydroxytabersonine and tabersonine epoxide.
(c) Co-expression of T16H2, 16OMT, T19H and TAT in yeast fed with tabersonine ultimately lead to the formation of the new-to-*C. roseus* 16-methoxy-19-acetyl-tabersonine. In (b) and (c), arrows highlight the formation of intermediates and final products. [Colour figure can be viewed at wileyonlinelibrary.com].

© 2018 The Authors

the 17-*O*-acetylated norajmaline from *R. serpentina* and strictly requires a saturated 19-20 bond (Polz *et al.*, 1987). This substrate preference supports the accumulation profile of 19-*O*-acetylated tabersonine derivatives in the analyzed root samples since only echitovenine, resulting from minovincinine acetylation, was detected (Figure 4(b)).

While we were not able to confirm TAT functions using VIGS due to the inefficiency of this approach in roots (Figure S13), its high catalytic efficiency *in vitro* and its capacity to work *in planta* and in other distinct heterologous organisms (Table 1 and Figure 5, Figure S13 and Figure S14) collectively provide strong evidence of a prominent role for TAT in MIA biosynthesis in *C. roseus* roots. Accordingly, TAT gene expression profile is very similar to T19H and follows tabersonine root metabolite accumulation (Figure 4(a, b)) in accordance with the fact that genes belonging to a same pathway often exhibit similar expression profiles correlated to MIA accumulation (Besseau *et al.*, 2013; Dugé Bernonville *et al.*, 2015; Parage *et al.*, 2016).

Combinatorial biosynthesis of *C. roseus* root-type MIAs in yeast

The identification of TAT enabled development of the metabolic engineering of *C. roseus* root-type MIAs in yeast. Feeding tabersonine, vincadifformine or hörhammericine as starting substrates to engineered yeast yielded known as well as unnatural MIAs (Figures 6, S16 and S17). First, by combining enzymes from the vindoline (leaf) and root-alkaloid pathways, we showed that regiospecific modifications of tabersonine may also involve conformational specificities of close positions since only the distal C16 hydroxylation/methylation and C2–C3 epoxidation or C16 hydroxylation/methylation and C19 hydroxylation/acetylation can occur simultaneously on the same molecule. This yeast engineering approach also demonstrated that substrate promiscuities of T16H2, 16OMT, T3O, T19H and TAT allow new opportunities to synthesize unusual or new-to-nature compounds. While echitoveniline, 16-methoxyechitoveniline or 16-methoxyechitovenidine have already been identified in leaves and fruits of *Alstonia venenata*, the synthesis of 16-methoxyechitovenine resulting from the combination of T16H2, 16OMT, T19H and TAT has never been observed in nature (Majumder *et al.*, 1979; Figure S16). Interestingly, precursors have been described in *Vinca minor* including ervinceine (16-methoxyvincadifformine) or minovincinine (thus hydroxylated at C19) but no mixed forms or acetylated compounds have been observed, likely because of the lack of a close ortholog of TAT in this plant (Demessie *et al.*, 2017; closest ortholog in *Vinca minor* share around 30% identify with TAT). By contrast, the absence of these compounds in *C. roseus* plants largely results from the organ-specificity of gene expression of T16H2/16OMT and T19H/TAT in leaves and roots, respectively. However, cell suspension cultures have been shown to accumulate 16-methoxy-19-acetyltabersonine, 16-methoxy-19-hydroxytabersonine or lochnerinine (16-methoxylochnericine) as a consequence of a possible alteration of gene expression profile in dedifferentiated cells (Kurz *et al.*, 1980; Kutney *et al.*, 1980). This is also potentially applicable to 16-methoxy-19-acetylhörhammercine and to the new compounds resulting from T3O activity such as hörhammericine epoxide and vincadifformine epoxide (Figure S17(a)). Further elucidation of the MIA biosynthetic pathway and its organization at the cellular and subcellular levels in *C. roseus* and other MIA-producing Apocynaceae will contribute to expand the tool-box for MIA genetic engineering. The combinatorial biosynthesis of MIAs related to tabersonine would allow quick access to diverse analogs for biological evaluation. For example, tabersonine has been reported to be a lead compound in the treatment of Alzheimer's disease by disrupting amyloid beta (Aβ) fibrils and ameliorates Aβ aggregate-induced cytotoxicity (Kai *et al.*, 2015). In addition, more highly oxidized tabersonine congeners such as the jerantinines have been shown to possess potent anti-cancer activities and merit further study (Lim *et al.*, 2008; Frei *et al.*, 2013; Chung *et al.*, 2017).

In conclusion, we identified in this work a new BAHD enzyme that catalyzes acetylation of root-type tabersonine derivatives in *C. roseus*, thus allowing the refinement of the MIA biosynthetic pathway and also the opportunity to establish the metabolic engineering of periwinkle root-type MIAs ultimately leading to the synthesis of unnatural MIAs. This discovery enables controlled decorations of vincadifformine, tabersonine or hörhammericine to enrich the panel of compounds that can be used for downstream chemical modifications as described with mutants of MIA biosynthetic enzymes (Bernhardt *et al.*, 2007) or to broaden their intrinsic pharmaceutical properties as previously described for vincadifformine derivatives (Mustopha *et al.*, 2006; Cao *et al.*, 2012).

EXPERIMENTAL PROCEDURES

Chemicals

Tabersonine was purchased from ChromaDex (USA). Hörhammericine was purified from *C. roseus* according to Giddings *et al.* (2011). Vincadifformine was prepared by the hydrogenation of tabersonine as described in Zhao and Andrade (2013). Acetyl-CoA and CoA were purchased from Sigma while other CoA-esters were chemically prepared according to previously published methods (Stöckigt and Zenk, 1975; Negrel and Smith, 1984; Elejalde-Palmett *et al.*, 2015)..

Plant growth conditions

C. roseus (cultivar Apricot Sunstorm) were grown in a greenhouse at 28°C under a 16h light/8h dark cycle and were used for all experiments except VIGS assays that were conducted on the Little

© 2018 The Authors

Bright Eyes cultivar as described in Carqueijeiro *et al.* (2015). Hairy roots were propagated as described in Courdavault *et al.* (2005). *N. benthamiana* were cultivated in a greenhouse at 24°C with a photoperiod of 16 h/8 h light/dark cycle.

Development of water-induced adventitious roots

Water-induced adventitious roots were generated by immersing freshly cut stems of 6–8-week plantlets (Apricot Sunstorm cultivar). Leaves from the last 10 cm of stem were removed before immersion whereas upstream leaves were maintained to allow photosynthesis. Plantlets were placed in greenhouse (28°C, 16 h/8 h photoperiod) and water was changed every 3 days. First adventitious roots begin to develop on stems almost 5 days after immersion and reach a 5-cm length around 2 weeks later. Apical parts of roots (1 cm) were harvested for RNA sequencing and metabolites quantification.

RNA-seq procedures

RNAs were extracted using TRIzol (Life Technologies) according to Dugé de Bernonville *et al.* (2017). RNA-seq library preparation and high-throughput sequencing were performed by Eurofins using Illumina HiSeq 2000/2500 with chemistry v3.0 in the paired mode. The adventitious root sample was deposited on EBI ENA under accession number ERR2112587 (study PRJEB22378).

De novo transcriptome assembly and abundance estimation

Individual root transcriptomes were assembled with Trinity v2.1.1 after applying an *in silico* normalization step (with a max_cov value of 50) (Haas *et al.*, 2013) as described in the method section of Figure S3.

Co-expression of T19H and BAHDs in yeast for identification of tabersonine derivative acetyltransferase activity

Full length open reading frames of T19H, MAT, CRO_T005210, TAT (CRO_T005215), CRO_T022100, CRO_T020281 and DAT were amplified using specific pairs of primers (Table S4). These primer couples have been designed to include restriction sites at their extremities to allow cloning of the T19H amplicon into pYEDP60, MAT, TAT (CRO_T005215) and CRO_T022100 into pESC-HIS and DAT, CRO_T005210 and CRO_T020281 into pESC-TRP. Recombinant plasmids were independently used to transform the *S. cerevisiae* strain WAT11 expressing the *A. thaliana* NADPH P450 reductase 1 (Pompon *et al.*, 1996). Each BAHD expressing vector was also co-transformed with the T19H expressing vector. Yeasts were grown in 10 mL of CSM medium (Yeast Nitrogen Base 0.67%, dextrose 2%, drop-out mix without adenine and uracil 0.05%) until reaching the stationary phase of culture and prior being harvested by centrifugation. Protein expression was induced by cultivating the harvested yeast in 50 mL of YPGal medium (2% bacto peptone, 1% yeast extract, and 2% galactose) for 6 h as described in Parage *et al.* (2016).

BAHD functional assays in yeast and large scale product synthesis

BAHD functional assays in yeast were performed by feeding 175 μl of galactose-induced recombinant yeast strains with 125 μM or 500 μM of tabersonine, vincadifformine (for strains expressing T19H and one BAHD), hörhammericine and deacetylvindoline (for strains expressing a BAHD without T19H), during 16 h at 30°C under continuous shaking. Reactions were centrifuged (10 min; 5000 ***g***) and supernatants were collected before adding three methanol volumes. Following homogenization with vortex, reactions were centrifuged (15 min; 25 000 ***g***) before subsequent UPLC-MS analysis. For large scale product synthesis, 30 mL of the T19H/TAT expressing yeast strain were grown, induced and fed with 2 mg of *tabersonine* during 24 h at 30°C. Following centrifugation (10 min; 5000 ***g***), supernatant was collected and alkalinized to pH 9 using NaOH. One volume of dichloromethane was then added and the resulting solution homogenized with vigorous shaking for phase separation. The organic phase was collected and evaporated. The extraction of alkaloids from the alkalinized supernatant was performed twice. Reaction products were finally re-suspended in methanol before analysis.

Production of recombinant TAT and MAT in *E. coli* and steady-state enzyme kinetics

Recombinant TAT and MAT were produced by amplifying their coding sequences using primers T005215-Bam-for/T005215-Bam-rev and MAT-Bam-for/MAT-Bam-rev (Table S4) and cloning the resulting polymerase chain reaction (PCR) products into pQE-30 (Qiagen) and pRSET-A (Invitrogen), respectively. Recombinant plasmid was co-transformed in *E. coli* BL21(DE3) with pUBS520 expressing the rare arginine encoding codons (AGA, AGG). Transformed cells were cultivated until exponential growth ($Abs_{595\ nm}$ = 0.5) before inducing protein expression by adding 1 mM IPTG for 4 h at 28°C. Recombinant proteins were purified using a Co^{2+} matrix according to the manufacturer's protocol (Talon Resin metal ion, Clontech) and subsequently concentrated and dialyzed against phosphate buffer (100 mM pH 7.5) using centricon (30 kDa cut-off, Millipore). 10% glycerol was finally added before freezing aliquoted protein in liquid nitrogen. Enzymatic assays were conducted at 30°C in 20 μL final volume containing HEPES buffer (100 mM pH 7.6 supplemented with 2 mM of ascorbic acid) and various amounts of acceptor/donor substrates. Kinetic parameters were measured using 1 μg of recombinant MAT/mMAT for 2 min or 0.1 μg of recombinant TAT/mTAT for 1 min with increasing amounts of 19-hydroxytabersonine, minovincinine, hörhammericine or deacetylvindoline (0, 1,2, 5, 10, 100, 250 or 500 μM) in the presence of 500 μM acetyl-CoA, and increase amounts of acetyl-CoA (0, 0.1, 0.5, 1, 10, 100, 500 or 800 μM) in the presence of 300 μM of minovincinine. Additional substrates were tested using 1 μg of recombinant proteins and 20 min incubation, including caffeic acid, quercetin, spermidine, and naringenin (10 or 200 μM) as acceptors in the presence of 500 μM acetyl-CoA. CoA donors were also tested by incubating 1 μg of recombinant proteins with sinapoyl-CoA (60 μM), feruloyl-CoA (60 μM), and cinnamoyl-CoA (100 μM), in the presence of 300 μM of minovincinine. Finally, deacetyltransferase activities of the recombinant proteins were assayed with 19-*O*-acetyltabersonine (0, 50, or 500 μM) in the presence of 500 μM CoA. For each assay, reactions were stopped by adding one volume of methanol followed by vigorous shaking. For UPLC-MS analyses, four volumes of 0.1% formic acid in water were added. Solutions were vortexed and centrifuged for 10 min at 16 000 ***g*** before collecting 5 μL of the supernatant for injection.

UPLC-MS analyses

UPLC-MS analyses were conducted using equipment and condition described in Parage *et al.* (2016). Data collection was carried in selected ion monitoring (SIM) mode for the following compounds:

© 2018 The Authors

tabersonine m/z 337 RT = 14.4 min, 16-hydroxytabersonine m/z 353 RT = 8.4 min, tabersonine 2,3-epoxide m/z 353 RT = 11.4 min, 19-hydroxytabersonine m/z 353 RT = 6.5 min, 16-methoxytabersonine m/z 367 RT = 12.03 min, 16-methoxy-19-hydroxytabersonine m/z 383 RT = 7.66 min, 16-methox-19-acetyltabersonine m/z 425 RT =14.6 min, vincadifformine m/z 339 RT = 11.40 min, minovincinine m/z 355 RT = 5.56 min, echitovenine m/z 397 RT = 10.12 min, vincadifformine 2,3-epoxide m/z 355 RT = 11.67 min, ervinceine (syn: 16-methoxyvincadifformine) m/z 369 RT = 12.5 min, 16-methoxyechitovenine m/z 427 RT = 7.24 min, hörhammericine m/z 369 RT = 5.7 min, 19-acetylhörhammericine m/z 411 RT = 12.2 min, 16-methoxy-19-acetylhörhammericine m/z 441 RT = 6.1 min, 19-acetyltabersonine m/z 395 RT = 15.6 min, 16-methoxytabersonine epoxide/imine alcohol m/z 383 RT = 8.89 min, 16-methoxyvincadifformine epoxide m/z 385 RT = 8.34 min, hörhammericine epoxide m/z 385 RT = 5.4, deacetylvindoline m/z 415 RT = 12.4, vindoline m/z 457 RT = 15.4, quercetin m/z 301 (es-) RT = 11.1, naringenin m/z 271 (es-) RT = 12.28, cyanidin m/z 287 (es-) RT = 10.43, caffeic acid m/z 179 (es-) RT = 3.87, spermidine m/z 146 (es-) RT = 4.53.

Nuclear magnetic resonance spectroscopy

^{1}H NMR, ^{1}H-^{1}H COSY, HSQC and HMBC spectra were recorded on an Avance III HD 700 NMR spectrometer (Bruker-Biospin, Karlsruhe, Germany) at 300 K using a 1.7 mm TCI CryoProbe™. Spectra were referenced to the residual solvent signal at δ_H 3.31 and δ_C 49.15. Coupling constants are in Hertz (Hz).

Gene expression analysis (real-time RT-PCR)

Expressions of T19H, TAT, MAT and DAT were analyzed by real-time RT-PCR according to Parage *et al.* (2016) and Liscombe and O'Connor (2011), using primers compiled in Table S4, *RPS9* and *EF1*α as endogenous reference genes and retro-transcribed RNAs from different *C. roseus* organs (including roots, stems, young and mature leaves – Apricot Sunstorm cultivar; adventitious roots and hairy roots).

Detection of proteins through western blot analysis

Proteins were extracted by grounding plant and yeast samples in liquid nitrogen and thawing in cold lysis buffer containing 100 mM Tris pH 7.5, 1 mM EDTA, 1 mM DTT, 1 mM PMSF, 1 mM $MgCl_2$ and protease inhibitors cocktail (Complete EDTA-free, Roche). Cell debris were removed by centrifugation at 25 000 ***g*** for 25 min at 4°C and protein concentrations were determined with Bradford reagent (Bio-Rad) before electrophoretic separation of 20 μg of proteins of each sample on SDS-PAGE (10%). Proteins were detected by western blot analysis according to Oudin *et al.* (2007) using the anti-GFP or anti-flag antibodies and the anti-mouse immunoglobulin alkaline phosphatase conjugate, diluted as recommended by the supplier (Covalab).

Analysis of TAT and MAT activities through agroinfiltration and leaf disk assays

Leaf disc assays were performed according to Höfer *et al.* (2013) with some modifications. For transient expression of TAT and MAT in *N. benthamiana* leaves, TAT and MAT coding sequences were first amplified using primers TAT–YFP-for/TAT–YFP-rev and MAT–YFP-for/MAT–YFP-rev (Table S4), digested by *Spe*I and cloned into the binary vector pCAMBIA1302 to express the TAT–GFP and MAT–GFP fusion proteins. *Agrobacterium tumefaciens* strain GV3101 transformed with recombinant or empty vectors were co-infiltrated with *A. tumefaciens* transformed with pBin-P19 in young leaves of 5-week-old *N. benthamiana* plants. At 5 days post-infiltration, the presence of the proteins (GFP, MAT–GFP and TAT–GFP) was confirmed by GFP fluorescence monitoring as described in subcellular localization studies. Two centimeter diameter discs (around 0.15 to 0.3 g) were excised from the infiltrated leaves and placed in 10 mL 100 mM HEPES buffer pH 7.6 containing ascorbic acid 2 mM, acetyl-CoA 500 μM and minovincinine 300 μM, exposed to vacuum (50 mBar), and placed in a semi-dry Petri dish, for 120 min or 720 min in the dark at 24°C. Leaf discs were than lyophilized and alkaloids extracted and quantified by LC-MS as described above.

Combinatorial synthesis of MIAs through co-expression of leaf and root MIA biosynthetic enzymes in yeast

Bioconversions of tabersonine, vincadifformine and hörhammericine into unusual or new-to-nature compounds were achieved through co-expression of leaf and roots MIA biosynthetic enzymes in yeast. For these experiments, TAT and T19H cDNAs were subcloned into the *Spe*I and *BamH*I restriction sites of the pESC-TRP yeast expression vector (pESC-TRP-T19H/TAT), respectively, after amplification of their coding sequences using primers compiled in Table S4. pESC-TRP-TAT and pESC-TRP-T19H plasmids were also created accordingly. 16OMT and tabersonine 3-oxidase (T3O) were amplified with primers 16OMT-for/16OMT-rev and T3O-for/T3O-rev (Table S4) and cloned into the *BamH*I or *Spe*I restriction sites of pESC-LEU to generate the pESC-LEU-16OMT and the pESC-LEU-T3O vectors. Both cDNA were also cloned into a same plasmid to generate pESC-LEU-16OMT/T3O. T16H2 was expressed using the pYeDP60-T16H2 plasmid as described in Besseau *et al.* (2013). Recombinant plasmids were transformed into the WAT11 yeast strain to express T3O alone (pESC-LEU-T3O vector); T19H and T3O (pESC-TRP-T19H; pESC-LEU-T3O vectors); T16H2, 16OMT and T3O (pYeDP60-T16H2, pESC-LEU-16OMT/T3O vectors); T16H2, 16OMT and TAT (pYeDP60-T16H2, pESC-LEU-16OMT and pESC-TRP-TAT vectors); T16H2, 16OMT, T19H and TAT (pYeDP60-T16H2, pESC-LEU-16OMT and pESC-TRP-T19H/TAT vectors). Transformed yeasts were grown in 10 mL of CSM medium (Yeast Nitrogen Base 0.67%, dextrose 2%, drop-out mix without adenine and uracil 0.05% for pYeDP60 plasmid selection, without tryptophan for pESC-TRP plasmid selection or leucine for pESC-LEU plasmid selection) and induced as described above. Bioconversions were achieved by feeding recombinant yeasts with 125 μM of tabersonine, vincadifformine or hörhammericine and quantified as described in the BAHD functional assays in yeast section.

ACCESSION NUMBERS

GenBank accession number of TAT is KU821123. Accession numbers of the adventitious root transcriptomic resource is ERR2112587.

ACKNOWLEDGEMENTS

We gratefully acknowledge support from the 'Région Centre-Val de Loire' (France, ABISAL grant, BioPROPHARM Project – ARD2020 Biomédicaments and CatharSIS program) and from the University of Tours. IC was financed by a Post-doctoral fellowship from Région Centre Val de Loire. We thank Marie-Antoinette Marquet, Evelyne Danos, and Cédric Labarre (EA2106 BBV) for help in maintaining cell cultures and plants; Emeline Marais and Céline Melin (EA2106 BBV) for valuable technical assistance and the Fédération CaSciModOT for access to the Région Centre computing grid. We also thank Sybille Lorenz (Max-Planck-Institute) for HRMS measurement. R. Andrade and C. Teijaro acknowledge the National Science Foundation for funds (CHE-1362461 and DEG-12262).

© 2018 The Authors

CONFLICT OF INTEREST

The authors declare no conflict of interest.

AUTHOR CONTRIBUTIONS

I.C. performed BAHD acyltransferase assays in yeast/*in planta*, biochemical characterization of enzymes, VIGS analysis, subcellular localization studies and combinatorial synthesis of alkaloids; T.D.D.B. achieved transcriptomics and genomics analyses; A.L., K.B. performed UPLC-MS analyses; T.T.D. purified hörhammericine and assisted in enzyme characterization; C.T., R.B.A. synthesized vincadifformine; A.M. contributed to subcellular localizations; C.P., B.S. performed NMR analyses; A.O., G.G. carried out gene expression analyses; S.B. synthesized CoA ester donors and performed enzyme mutations; N.P. assisted in combinatorial synthesis of alkaloids; M.C., N.G.G, L.A. contributed to biochemical characterization of enzymes; B.St-P assisted in the characterization of TAT and MAT *in vivo* activities and in the supervision of this work; S.E.O. contributed to identification of TAT, conception of this work and experiment design. V.C. conceived, supervised this study and wrote the manuscript.

SUPPORTING INFORMATION

Additional Supporting Information may be found in the online version of this article.

Figure S1. Controls of MAT activity in yeast.

Figure S2. Distribution of tabersonine derivative 19-*O*-acetyltransferase and deacetylvindoline transferase activities and MIAs in *C. roseus* organs and formation of induced adventitious roots used for RNA sequencing.

Figure S3. Expression levels of candidate MIA genes obtained from full organ and paired-end sequenced samples, with pre-existing transcriptomic resources (a) and the leaf and adventitious root data (Apricot Sunstorm cultivar) generated in this work (b).

Figure S4. Characterization of pre-existing *C. roseus* root transcriptome and adventitious root transcriptome generated in this work.

Figure S5. Genomic organization of the BAHD candidates on scaffolds 3067490 (in red) and 3060125 (in purple).

Figure S6. Phylogenic tree of the plant BAHD acyltransferases.

Figure S7. Alignment of the candidate BAHD, DAT and MAT deduced amino-acid sequences.

Figure S8. Subcellular localization of CRO_T005210.

Figure S9. Screening for root tabersonine derivatives and deacetylvindoline acetyltransferase activities of selected BAHD candidates, MAT and DAT.

Figure S10. TAT catalyzes the synthesis of 19-O-acetyltabersonine.

Figure S11. Purification of the recombinant MAT, TAT (a), mutated MAT (mMAT) and TAT (mTAT) (b) analyzed by SDS-PAGE and comparison of acetyltransferase (c) or deacetyltransferase (d) activities.

Figure S12. T19H transmembrane helix prediction and subcellular localization of T19H, MAT and TAT.

Figure S13. Virus-induced gene silencing of TAT or PDS in *C. roseus* performed through biolistic transformation of whole plantlets.

Figure S14. MAT *in vivo* inactivity does not result from altered subcellular localization or limited substrate availability in yeast.

Figure S15. MS/MS Spectrum of the [M+H]+ ion from 16-methoxy-19-acetyltabersonine.

Figure S16. Gathering enzymes from roots and leaves in yeast allows conversion of vincadifformine.

Figure S17. Gathering enzymes from roots and leaves in yeast allows conversion of hörhammericine.

Table S1. Lists of transcripts identified with root related Gene Ontology terms in root samples from NIPGR and Apricot Sunstorm (this study).

Table S2. Identity (%) between the newly identified BAHD candidates, DAT and MAT at the amino-acid level.

Table S3. BAHD accession numbers.

Table S4. Primers used in this study.

REFERENCES

Bayer, A., Ma, X. and Stöckigt, J. (2004) Acetyltransfer in natural product biosynthesis–functional cloning and molecular analysis of vinorine synthase. *Bioorg. Med. Chem.*, **12**, 2787–2795. https://doi.org/10.1016/j.bmc.2004.02.029

Bernhardt, P., McCoy, E. and O'Connor, S.E. (2007) Rapid identification of enzyme variants for reengineered alkaloid biosynthesis in periwinkle. *Chem. Biol.*, **14**, 888–897. https://doi.org/10.1016/j.chembiol.2007.07.008

Besseau, S., Kellner, F., Lanoue, A. *et al.* (2013) A pair of tabersonine 16-hydroxylases initiates the synthesis of vindoline in an organ-dependent manner in *Catharanthus roseus*. *Plant Physiol.*, **163**, 1792–1803. https://doi.org/10.1104/pp.113.222828

Brown, S., Clastre, M., Courdavault, V. and O'Connor, S.E. (2015) *De novo* production of the plant-derived alkaloid strictosidine in yeast. *Proc Natl Acad Sci U S A.*, **112**, 3205–3210. https://doi.org/10.1073/pnas.1423555112

Cao, P., Liang, Y., Gao, X., Li, X.M., Song, Z.Q. and Liang, G. (2012) Monoterpenoid indole alkaloids from Alstonia yunnanensis and their cytotoxic and anti-inflammatory activities. *Molecules*, **17**, 13631–13641. https://doi.org/10.3390/molecules171113631

Carqueijeiro, I., Masini, E., Foureau, E. *et al.* (2015) Virus-induced gene silencing in *Catharanthus roseus* by biolistic inoculation of tobacco rattle virus vectors. *Plant Biol., (Stuttg)*, **17**, 1242–1246. https://doi.org/10.1111/plb.12380

Chung, F.F., Tan, P.F., Raja, V.J. *et al.* (2017) Jerantinine A induces tumor-specific cell death through modulation of splicing factor 3b subunit 1 (SF3B1). *Sci. Rep.*, **7**, 42504. https://doi.org/10.1038/srep42504

Courdavault, V., Burlat, V., St-Pierre, B. and Giglioli-Guivarc'h, N. (2005) Characterisation of CaaX-prenyltransferases in *Catharanthus roseus*: relationships with the expression of genes involved in the early stages of monoterpenoid biosynthetic pathway. *Plant Sci.*, **168**, 1097–1107. https://doi.org/10.1016/j.plantsci.2004.12.010

Courdavault, V., Papon, N., Clastre, M., Giglioli-Guivarc'h, N., St-Pierre, B. and Burlat, V. (2014) A look inside an alkaloid multisite plant: the Catharanthus logistics. *Curr. Opin. Plant Biol.*, **19**, 43–50. https://doi.org/10.1016/j.pbi.2014.03.010

D'Auria, J.C. (2006) Acyltransferases in plants: a good time to be BAHD. *Curr. Opin. Plant Biol.*, **9**, 331–340. https://doi.org/10.1016/j.pbi.2006.03.016

Demessie, Z., Woolfson, K.N., Yu, F., Qu, Y. and De Luca, V. (2017) The ATP binding cassette transporter, VmTPT2/VmABCG1, is involved in export of the monoterpenoid indole alkaloid, vincamine in *Vinca minor* leaves. *Phytochemistry*, **140**, 118–124. https://doi.org/10.1016/j.phytochem.2017.04.019

Dugé Bernonville, T., Foureau, E., Parage, C. *et al.* (2015) Characterization of a second secologanin synthase isoform producing both secologanin and secoxyloganin allows enhanced *de novo* assembly of a *Catharanthus roseus* transcriptome. *BMC Genom.*, **16**, 619. https://doi.org/10.1186/s12864-015-1678-y

Dugé de Bernonville, T., Carqueijeiro, I., Lanoue, A. *et al.* (2017) Folivory elicits a strong defense reaction in *Catharanthus roseus*: metabolomic and transcriptomic analyses reveal distinct local and systemic responses. *Sci. Rep.*, **7**, 40453. https://doi.org/10.1038/srep40453

© 2018 The Authors

Elejalde-Palmett, C., de Bernonville, TD., Glévarec, G., Pichon, O., Papon, N., Courdavault, V., St-Pierre, B., Giglioli-Guivarc'h, N., Lanoue, A. and Besseau, S. (2015) Characterization of a spermidine hydroxycinnamoyltransferase in Malus domestica highlights the evolutionary conservation of trihydroxycinnamoyl spermidines in pollen coat of core Eudicotyledons. *J. Exp. Bot.*, **66**, 7271–7285. https://doi.org/10.1093/jxb/erv423

Ferreres, F., Pereira, D.M., Valentão, P., Oliveira, J.M., Faria, J., Gaspar, L., Sottomayor, M. and Andrade, P.B. (2010) Simple and reproducible HPLC-DAD-ESI-MS/MS analysis of alkaloids in *Catharanthus roseus* roots. *J. Pharm. Biomed. Anal.*, **51**, 65–69. https://doi.org/10.1016/j.jpba.2009.08.005

Frei, R., Staedler, D., Raja, A., Franke, R., Sasse, F., Gerber-Lemaire, S. and Waser, J. (2013) Total synthesis and biological evaluation of jerantinine E. *Angew. Chem. Int. Ed. Engl.*, **52**, 13373–13376. https://doi.org/10.1002/anie.201305533

Giddings, L.A., Liscombe, D.K., Hamilton, J.P., Childs, K.L., DellaPenna, D., Buell, C.R. and O'Connor, S.E. (2011) A stereoselective hydroxylation step of alkaloid biosynthesis by a unique cytochrome P450 in *Catharanthus roseus*. *J. Biol. Chem.*, **286**, 16751–16757. https://doi.org/10.1074/jbc.M111.225383

Haas, B.J., Papanicolaou, A., Yassour, M. *et al.* (2013) *De novo* transcript sequence reconstruction from RNA-seq using the Trinity platform for reference generation and analysis. *Nature Protoc.*, **8**, 1494–1512. https://doi.org/10.1038/nprot.2013.084

Höfer, R., Dong, L., André, F. *et al.* (2013) Geraniol hydroxylase and hydroxygeraniol oxidase activities of the CYP76 family of cytochrome P450 enzymes and potential for engineering the early steps of the (seco)iridoid pathway. *Metab. Eng.*, **20**, 221–232. https://doi.org/10.1016/j.ymben.2013.08.001

Kai, T., Zhang, L., Wang, X., Jing, A., Zhao, B., Yu, X., Zheng, J. and Zhou, F. (2015) Tabersonine inhibits amyloid fibril formation and cytotoxicity of Aβ(1-42). *ACS Chem. Neurosci.*, **6**, 879–888. https://doi.org/10.1021/acschemneuro.5b00015

Kellner, F., Kim, J., Clavijo, B.J. *et al.* (2015a) Genome-guided investigation of plant natural product biosynthesis. *Plant J.*, **82**, 680–692. https://doi.org/10.1111/tpj.12827

Kellner, F., Geu-Flores, F., Sherden, N.H., Brown, S., Foureau, E., Courdavault, V. and O'Connor, S.E. (2015b) Discovery of a P450-catalyzed step in vindoline biosynthesis: a link between the aspidosperma and eburnamine alkaloids. *Chem. Commun. (Camb.)*, **51**, 7626–7628. https://doi.org/10.1039/C5CC01309G

Kurz, W.G.W., Chatson, K.B., Constabel, F., Kutney, J.P., Choi, L.S.L., Kolodziejczyk, P., Sleigh, S.K., Stuart, K.L. and Worth, Brian R. (1980) Alkaloid production in *Catharanthus roseus* cell cultures: initial studies on cell lines and their alkaloid content. *Phytochemistry*, **19**, 2583–2587. https://doi.org/10.1016/S0031-9422(00)83923-0

Kutney, J.P., Choi, L.S., Kolodziejczyk, P., Sleigh, S.K., Stuart, K.L., Worth, B.R., Kurz, W.G.W., Chatson, K.B. and Constabel, F. (1980) Alkaloid production in *Catharanthus roseus* cell cultures: isolation and characterization of alkaloids from one cell line. *Phytochemistry*, **19**, 2589–2595. https://doi.org/10.1016/S0031-9422(00)83924-2

Laflamme, P., St-Pierre, B. and de Luca, V. (2001) Molecular and biochemical analysis of a Madagascar periwinkle root-specific minovincinine-19-hydroxy-O-acetyltransferase. *Plant Physiol.*, **125**, 189–198. https://doi.org/10.1104/pp.125.1.189

Levac, D., Murata, J., Kim, W.S. and De Luca, V. (2008) Application of carborundum abrasion for investigating the leaf epidermis: molecular cloning of *Catharanthus roseus* 16-hydroxytabersonine-16-O-methyltransferase. *Plant J.*, **53**, 225–236.

Lim, K.H., Hiraku, O., Komiyama, K. and Kam, T.S. (2008) Jerantinines A-G, cytotoxic Aspidosperma alkaloids from *Tabernaemontana corymbosa*. *J. Nat. Prod.*, **71**, 1591–1594. https://doi.org/10.1021/np800435c

Liscombe, DK. and O'Connor, SE. (2011) A virus-induced gene silencing approach to understanding alkaloid metabolism in *Catharanthus roseus*. *Phytochemistry*. **72**, 1969–1977. https://doi.org/10.1016/j.phytochem.2011.07.001

Luo, J., Nishiyama, Y., Fuell, C. *et al.* (2007) Convergent evolution in the BAHD family of acyl transferases: identification and characterization of anthocyanin acyl transferases from *Arabidopsis thaliana*. *Plant J.*, **50**, 678–695. https://doi.org/10.1111/j.1365-313X.2007.03079.x

Ma, X., Koepke, J., Panjikar, S., Fritzsch, G. and Stöckigt, J. (2005) Crystal structure of vinorine synthase, the first representative of the BAHD superfamily. *J. Biol. Chem.*, **280**, 13576–13583. https://doi.org/10.1074/jbc.M414508200

Magnotta, M., Murata, J., Chen, J. and De Luca, V. (2007) Expression of deacetylvindoline-4-O-acetyltransferase in *Catharanthus roseus* hairy roots. *Phytochemistry*, **68**, 1922–1931. https://doi.org/10.1016/j.phytochem.2007.04.037

Majumder, P.L., Joardar, S., Chanda, T.K., Dinda, B.N., Banerjee, M., Ray, A.B., Varenne, P. and Das, B.C. (1979) Structures and absolute stereochemistry of (-)-echitoveniline,(-)-11-methoxyechitoveniline and (-)-11-methoxyechitovenedine—new indole alkaloids of *Alstonia venenata* R Bv. *Tetrahedron*, **35**, 1151–1157. https://doi.org/10.1016/S0040-4020(01)93738-X

Miettinen, K., Dong, L., Navrot, N. *et al.* (2014) The seco-iridoid pathway from *Catharanthus roseus*. *Nat. Commun.*, **5**, 3606.

Mustopha, M., Mallié, M., Valentin, A. and Lewin, G. (2006) *In vitro* Antiplasmodial Activity and Cytotoxicity of Vincadifformine and Its Semisynthetic Derivatives. *I. J. Biotech.*, **11**, 878–883.

Negrel, J. and Smith, T. (1984) The Phosphohydrolysis of hydroxycinnamoylcoenzyme A thioesters in plant extracts. *Phytochemistry*, **23**, 31–34. https://doi.org/10.1016/0031-9422(84)83072-1

Oudin, A., Mahroug, S., Courdavault, V., Hervouet, N., Zelwer, C., Rodríguez-Concepción, M., St-Pierre, B. and Burlat, V. (2007) Spatial distribution and hormonal regulation of gene products from methyl erythritol phosphate and monoterpene-secoiridoid pathways in *Catharanthus roseus*. *Plant Mol. Biol.*, **65**, 13–30. https://doi.org/10.1007/s11103-007-9190-7

Parage, C., Foureau, E., Kellner, F. *et al.* (2016) Class II Cytochrome P450 Reductase Governs the Biosynthesis of Alkaloids. *Plant Physiol.*, **172**, 1563–1577. https://doi.org/10.1104/pp.16.00801

Polz, L., Schübel, H. and Stöckigt, J. (1987) Characterization of 2 beta (R)-17-O-acetylajmalan: acetylesterase–a specific enzyme involved in the biosynthesis of the Rauwolfia alkaloid ajmaline. *Z. Naturforsch. C.*, **42**, 333–342.

Pompon, D., Louerat, B., Bronine, A. and Urban, P. (1996) Yeast expression of animal and plant P450s in optimized redox environments. *Methods Enzymol.*, **272**, 51–64. https://doi.org/10.1016/S0076-6879(96)72008-6

Qu, Y., Easson, M.L., Froese, J., Simionescu, R., Hudlicky, T. and De Luca, V. (2015) Completion of the seven-step pathway from tabersonine to the anticancer drug precursor vindoline and its assembly in yeast. *Proc Natl Acad Sci U S A.*, **112**, 6224–6229. https://doi.org/10.1073/pnas.1501821112

Reumann, S., Chowdhary, G. and Lingner, T. (2016) Characterization, prediction and evolution of plant peroxisomal targeting signals type 1 (PTS1s). *Biochim. Biophys. Acta*, **1863**, 790–803. https://doi.org/10.1016/j.bbamcr.2016.01.001

Rodriguez, S., Compagnon, V., Crouch, N.P., St-Pierre, B. and de Luca, V. (2003) Jasmonate-induced epoxidation of tabersonine by a cytochrome P-450 in hairy root cultures of *Catharanthus roseus*. *Phytochemistry*, **64**, 401–409. https://doi.org/10.1016/S0031-9422(03)00269-3

Stavrinides, A., Tatsis, E.C., Foureau, E., Caputi, L., Kellner, F., Courdavault, V. and O'Connor, S.E. (2015) Unlocking the diversity of alkaloids in *Catharanthus roseus*: nuclear localization suggests metabolic channeling in secondary metabolism. *Chem. Biol.*, **22**, 336–341. https://doi.org/10.1016/j.chembiol.2015.02.006

Stavrinides, A., Tatsis, E.C., Caputi, L., Foureau, E., Stevenson, C.E., Lawson, D.M., Courdavault, V. and O'Connor, S.E. (2016) Structural investigation of heteroyohimbine alkaloid synthesis reveals active site elements that control stereoselectivity. *Nat. Commun.*, **15**, 12116. https://doi.org/10.1038/ncomms12116

Stöckigt, J. and Zenk, M.H. (1975) Chemical syntheses and properties of hydroxycinnamoyl-coenzyme A derivatives. *Z. Naturforschung - Section C Journal of Biosciences.*, **30**, 352–358.

St-Pierre, B., Laflamme, P., Alarco, A.M. and de Luca, V. (1998) The terminal O-acetyltransferase involved in vindoline biosynthesis defines a new class of proteins responsible for coenzyme A-dependent acyl transfer. *Plant J.*, **14**, 703–713. https://doi.org/10.1046/j.1365-313x.1998.00174.x

St-Pierre, B., Besseau, S., Clastre, M. *et al.* (2013) Deciphering the Evolution, Cell Biology and Regulation of Monoterpene Indole Alkaloids. In *New Light on Alkaloid Biosynthesis and Future Prospects – chap 3* (Giglioli-

© 2018 The Authors

Guivarc'h, N. ed). Amsterdam, The Netherlands: Elsevier, pp. 73–109. https://doi.org/10.1016/B978-0-12-408061-4.00003-1

Tuominen, L.K., Johnson, V.E. and Tsai, C.J. (2011) Differential phylogenetic expansions in BAHD acyltransferases across five angiosperm taxa and evidence of divergent expression among Populus paralogues. *BMC Genom.*, **12**, 236. https://doi.org/10.1186/1471-2164-12-236

Van der Heijden, R., Jacobs, D.I., Snoeijer, W., Hallard, D. and Verpoorte, R. (2004) The Catharanthus alkaloids: pharmacognosy and biotechnology. *Curr. Med. Chem.*, **11**, 607–628. https://doi.org/10.2174/0929867043455846

Westekemper, P., Wieczorek, U., Gueritte, F., Langlois, N., Langlois, Y., Potier, P. and Zenk, M.H. (1980) Radioimmunoassay for the determination of the indole alkaloid vindoline in Catharanthus. *Planta Med.*, **39**, 24–37. https://doi.org/10.1055/s-2008-1074900

Yu, X.H., Gou, J.Y. and Liu, C.J. (2009) BAHD superfamily of acyl-CoA dependent acyltransferases in Populus and Arabidopsis: bioinformatics and gene expression. *Plant Mol. Biol.*, **70**, 421–442. https://doi.org/10.1007/s11103-009-9482-1

Zhao, S. and Andrade, R.B. (2013) Domino Michael/Mannich/N-Alkylation Route to the Tetrahydrocarbazole Framework of Aspidosperma Alkaloids: concise Total Syntheses of (−)-Aspidospermidine, (−)-Tabersonine, and (−)-Vincadifformine. *J. Am. Chem. Soc.*, **135**, 13334–13337. https://doi.org/10.1021/ja408114u

© 2018 The Authors